

# Syntheses, Phase Behavior, Supramolecular Chirality, and Field-Effect Carrier Mobility of Asymmetrically End-Capped Mesogenic Oligothiophenes

Qingwei Meng,<sup>[a]</sup> Xiao-Hua Sun,<sup>[b]</sup> Zhengyu Lu,<sup>[a]</sup> Ping-Fang Xia,<sup>[b]</sup> Zehua Shi,<sup>[a]</sup>  
Dongzhong Chen,<sup>\*[a]</sup> Man Shing Wong,<sup>\*[b]</sup> Salem Wakim,<sup>[c]</sup> Jianping Lu,<sup>[c]</sup>  
Jean-Marc Baribeau,<sup>[c]</sup> and Ye Tao<sup>\*[c]</sup>

**Abstract:** A novel series of asymmetrically end-capped mesogenic oligothiophenes, with various oligothiophene core lengths, alkoxy tail lengths, and molecular polarities through introducing alkylsulfanyl or alkylsulfonyl functionalities as the terminal group, have been synthesized by palladium-catalyzed Suzuki cross-coupling and Kumada cross-coupling reactions as key steps. For the single end-capped oligothiophenes, C<sub>m</sub>O-Ar-OT(4)-H in which *m* = 10, 12, 14, 16, and 18, all of these oligomers exhibited a broad temperature range of highly ordered smectic E and enantiotropic nematic phases, apart from the one with the longest octadecyloxy tail. For the double end-capped series C<sub>10</sub>O-Ar-OT(*n*)-R, R = Ph-SC<sub>6</sub> or Ph-SO<sub>2</sub>C<sub>6</sub> in which *n* = 1, 2, 3, and 4, oligomers with more than one thiophene ring exhibited smectic A and smectic C phases, various crystal polymorphs and/or unusual low-tempera-

ture condensed phases. In the nonpolar, alkylsulfanylphenyl-substituted oligothiophene series, both the crystal/solid melting point and mesogenic clear point increased significantly with an increasing oligothiophene conjugation length. In the polar, alkylsulfonylphenyl-substituted oligothiophene series, all the oligomers showed increased melting points, but decreased mesogenic temperature intervals than those of their corresponding alkylsulfanyl counterparts. Remarkably, two different helical structures showing distinct striated textures or striped patterns were observed with a pitch of several to tens of micrometers under a polarized optical microscope upon

cooling from their preceding fluidic smectic phases. The unusual twisted smectic layer structures in the thin solid films exhibiting distinct supramolecular chirality of both handednesses, revealed by circular dichroism measurements, were further confirmed by XRD analyses characterized by a sharp layer reflection together with its higher orders and diffuse wide-angle scatterings. In addition, initial studies showed that the highly ordered smectic phase of the single end-capped oligothiophenes can be utilized to improve field-effect charge mobility. C<sub>10</sub>O-Ar-OT(4)-H showed a hole mobility of 0.07 cm<sup>2</sup>V<sup>-1</sup>s<sup>-1</sup> when deposited on octyltrichlorosilane-treated substrates at 140 °C and the on/off current ratios reached 5 × 10<sup>5</sup>; on the other hand, its mobility was only 8 × 10<sup>-3</sup> cm<sup>2</sup>V<sup>-1</sup>s<sup>-1</sup> on the same substrate when deposited at room temperature.

**Keywords:** liquid crystals · materials science · oligothiophenes · semiconductors · supramolecular chirality

[a] Dr. Q. Meng, Z. Lu, Z. Shi, Prof. Dr. D. Chen  
Key Laboratory of Mesoscopic Chemistry of Ministry of Education  
Department of Polymer Science and Engineering  
School of Chemistry and Chemical Engineering  
Nanjing University, Nanjing 210093 (China)  
Fax: (+86)25-8331-7761  
E-mail: cdz@nju.edu.cn

[b] Dr. X.-H. Sun, P.-F. Xia, Prof. Dr. M. S. Wong  
Department of Chemistry and Centre for Advanced  
Luminescence Materials  
Hong Kong Baptist University, Kowloon Tong  
Hong Kong (S.A.R. China)  
Fax: (+852)3411-7348  
E-mail: mswong@hkbu.edu.hk

[c] Dr. S. Wakim, Dr. J. Lu, Dr. J.-M. Baribeau, Dr. Y. Tao  
Institute for Microstructural Sciences (IMS)  
National Research Council of Canada  
Ottawa K1A 0R6 ON (Canada)  
Fax: (+1)613-990-0202  
E-mail: Ye.Tao@nrc-cnrc.gc.ca



Supporting information for this article is available on the WWW under <http://dx.doi.org/10.1002/chem.200802470>.

## Introduction

Oligothiophenes are an attractive class of organic semiconducting materials for applications as organic field-effect transistors (OFETs), organic light-emitting diodes (OLEDs), and photovoltaic (PV) cells because of their high solid-state ordering and good charge-carrier mobility.<sup>[1]</sup> Many nonsubstituted and  $\alpha,\omega$ -substituted oligothiophenes have been synthesized and applied for OFET applications recently.<sup>[2,3]</sup> Most of them exhibit good crystallinity and form polycrystalline films by vacuum deposition;<sup>[4]</sup> on the other hand, some symmetrically and asymmetrically dialkyl-substituted oligothiophenes exhibited mesophases and showed high charge-carrier mobility.<sup>[3]</sup> It is well known that for OFET applications, proper molecular alignment in the crystalline solid can give rise to high charge mobility and a low operating voltage; on the other hand, amorphous materials often give low charge mobility. Nevertheless, the use of polycrystalline materials for practical applications is often hampered by grain boundary effects, which cause electrically active localized states and dramatically decrease the charge-carrier mobility.<sup>[5]</sup> The potential of liquid-crystalline semiconductors for OFETs has recently been recognized because of their self-assembling nature, anisotropic transport, and high charge-carrier mobility.<sup>[6]</sup> Discotic<sup>[7]</sup> and smectic liquid crystals<sup>[3,8–11]</sup> are also known for their capabilities in self-healing structural defects and self-organizing into large structurally homogeneous domains, as well as exhibiting excellent charge-carrier transport properties. As a result, there has been considerable interest in exploring liquid-crystalline oligothiophenes for various optoelectronic applications. Most known mesogenic oligothiophenes are generally derived from the symmetrically disubstituted oligothiophenes with a structural motif of donor–oligothiophene–donor or acceptor–oligothiophene–acceptor, asymmetrically disubstituted donor–acceptor-type liquid-crystalline oligothiophene has rarely been reported.

In smectic liquid crystals, the charge-carrier mobility is mainly dependent on the molecular distance within a smectic layer, in which the calamitic molecules address and the charge carriers hop from one molecule to the other. It is desirable that the domain boundary effects in the smectic phases are very small.<sup>[9a,10]</sup> In principle, high carrier mobility could be achieved from a large  $\pi$ -conjugated system exhibiting highly ordered smectic mesophases; however, even enhanced intermolecular interactions between larger  $\pi$ -conjugated molecules usually result in crystallization and the above-mentioned polycrystalline boundary effects. An asymmetric molecular structure tends to reduce the transition temperature and extend the mesophase range in the liquid crystals.<sup>[3f,i]</sup> On the other hand, with an extension of  $\pi$  conjugation, the hybridized co-oligomers of thiophene and phenylene have been developed as a new class of light-emitting materials<sup>[12]</sup> and easily processable OFETs.<sup>[11,13]</sup> In addition, compared with their polymer analogues, well-defined oligomeric liquid crystalline semiconducting materials with high purity, precise chemical structure, and conjugation length

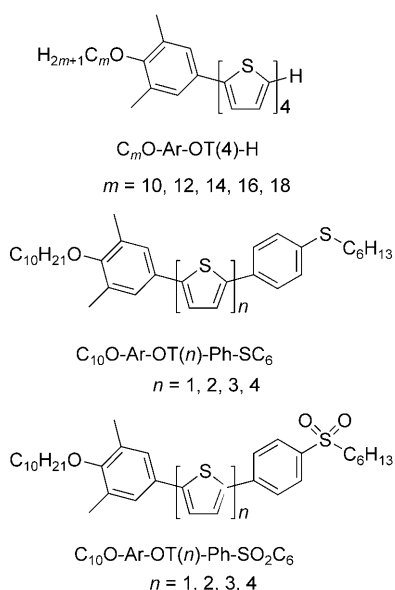
are of higher order and are solution processable; thus, they are considered to be realistic candidates for industrial applications as OFETs for cheap, large area, smart electronic devices.<sup>[9b,c,11,14]</sup>

Supramolecular chirality formed from the assembly of achiral molecules through noncovalent interactions is highly important and intriguing for its crucial role in biological phenomena, such as molecular recognition, as well as in information storage and potential applications in materials science.<sup>[15]</sup> Chiral symmetry breaking from achiral molecules is known to occur in controlled crystals,<sup>[15c]</sup> bent-core molecules,<sup>[15e,f,16]</sup> in a unique cooperative stereoregular arrangement or helical supramolecular organization through coordination with metal ions<sup>[17,18a,b]</sup> or through hydrogen bonding.<sup>[15d,h,18c,d]</sup> In addition to the interfacial constraint and the spontaneous overcrowded packing, the  $\pi$ - $\pi$  stacking between the rigid aromatic cores and the van der Waals interactions among the alkyl chains are considered to be important interactions for many robust supramolecular assemblies that give rise to the chiral helical superstructure.<sup>[18]</sup> Nanoscopic and mesoscopic order in  $\pi$ -conjugated systems is a topic of utmost importance, while the detailed understanding of the supramolecular interactions between the  $\pi$ -conjugated molecules is still one of the most challenging scientific research areas.<sup>[19]</sup>

We report herein the synthesis and investigation of thermotropic liquid-crystalline structures and properties of a novel series of asymmetrically end-capped oligothiophenes by means of modifying the oligothiophene core length, alkoxy tail length, and molecular polarity by introducing an alkylsulfanyl or alkylsulfonyl functionality as the terminal group. The general design principle of these new mesogens is based on a compromise between the order introduced by the  $\pi$ - $\pi$  stacking of the aromatic cores and the disorder caused by the flexible alkyl substituents.<sup>[3h–j]</sup> In the present studies, we explore two different strategies of tuning the liquid-crystal phase structure and transition temperatures. One is to systematically change the oligothiophene core length with predefined asymmetric end substituents, whereas the other is to alter the length of the alkoxy chain tethered to the predefined rigid core, arylene-capped quaterthiophene. All of these oligomers are components of three novel series of asymmetrically end-capped oligothiophenes as shown in Scheme 1. We have demonstrated for the first time that unusual layered condensed phases with supramolecular chirality have been achieved from some of the newly synthesized achiral double end-capped oligothiophenes upon cooling from their smectic phases. In addition, the initial OFET measurements on the single end-capped oligothiophenes with highly ordered smectic phases show high charge mobility.

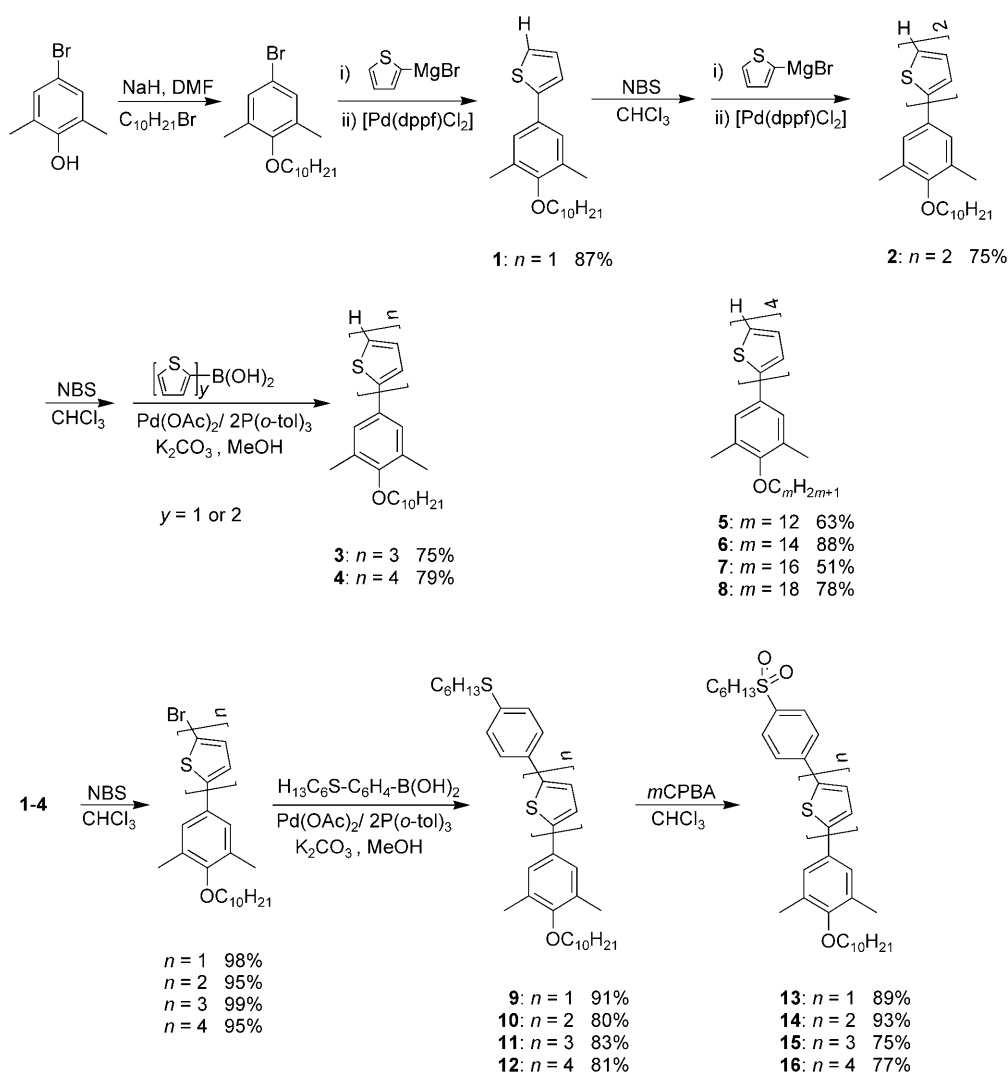
## Results and Discussion

**Synthesis:** The asymmetrically end-substituted oligothiophenes,  $C_mO-Ar-OT(n)-R'$  (Scheme 1), in which  $R' = H, Ph$



Scheme 1. Molecular structures of mesogenic oligothiophenes.

SC<sub>6</sub>, or Ph-SO<sub>2</sub>C<sub>6</sub> with various oligothiophene core lengths, alkoxy tail lengths, and molecular polarities through introducing alkylsulfanyl or alkylsulfonyl functionalities as the terminal group were synthesized by palladium-catalyzed Kumada cross-coupling and Suzuki cross-coupling reactions as key steps as shown in Scheme 2. Previously, the arylene end-capped quaterthiophene was synthesized by a linear approach using stepwise Kumada cross-couplings for chain-length extension.<sup>[20]</sup> To improve the operation and efficiency further, the convergent approach was developed to synthesize terthiophenyl and quaterthiophenyl skeletons by means of Suzuki cross-coupling reactions. The previously published protocols were followed for the synthesis of arylene end-capped thiophene **1** and bithiophene **2**. The palladium-catalyzed Suzuki cross-coupling of arylene end-capped bromothiophene or bromobithiophene with thiopheneboronic acid or bithiopheneboronic acid using Pd(OAc)<sub>2</sub>/2P(*o*-tol)<sub>3</sub> as a catalyst afforded arylene end-capped terthiophene **3** and quaterthiophene **4**, respectively, in good yields. By adopting the same synthetic approach and using various alkyl halides



Scheme 2. Synthesis of asymmetrically arylene end-capped oligothiophenes.

including dodecyl, tetradecyl, hexadecyl, and octadecyl bromides for the alkylation of 4-bromo-2,6-dimethylphenol, oligomer **5–8** ( $C_mO-Ar-OT(4)-H$ , in which  $m = 12, 14, 16,$  and  $18$ ) were prepared in good yields. The Suzuki cross-coupling of arylene end-capped bromooligothiophenes with 4-(hexylsulfanyl)phenylboronic acid, which was prepared by lithium–bromide exchange at  $-78^\circ\text{C}$  and quenching with trimethyl borate, afforded the corresponding asymmetrically disubstituted oligothiophenes, **9–12**,  $C_{10}O-Ar-OT(n)-Ph-SC_6$  in which  $n = 1–4$ , respectively. Subsequent oxidation of **9–12** with 3-chloroperbenzoic acid ( $m$ -CPBA) in  $CHCl_3$  gave the corresponding hexylsulfonylphenyl end-capped oligothiophenes, **13–16**,  $C_{10}O-Ar-OT(n)-Ph-SO_2C_6$  in which  $n = 1–4$ , respectively. All of the newly synthesized oligothiophenes were fully characterized by  $^1H$  and  $^{13}C$  NMR spectroscopy, high-resolution mass spectrometry, and elemental analysis and were found to be in good agreement with the expected structures.

**Thermal behavior and liquid-crystalline properties:** The thermal behavior and phase transitions of all of the oligothiophenes were initially examined by differential scanning calorimetry (DSC) and polarized optical microscopy

(POM). For easy comparison, these oligothiophenes,  $C_mO-Ar-OT(n)-R'$  could be divided into two sub-groups: the single end-capped series,  $C_mO-Ar-OT(4)-H$  in which  $m = 10, 12, 14, 16,$  and  $18$  and the double end-capped series,  $C_{10}O-Ar-OT(n)-R$ , in which  $R = Ph-SC_6$  or  $Ph-SO_2C_6$  and  $n = 1, 2, 3,$  and  $4$  (Scheme 1).

For the single end-capped oligothiophenes with a conjugating thiophene unit less than four, such as **2** and **3**, only a sharp crystal melting transition was observed in the DSC heating traces. On the other hand, quaterthiophenes **4–8** of the  $C_mO-Ar-OT(4)-H$  series exhibited rich thermal transitions and multiple mesogenic phases, which indicates a good balance of rigid core and flexible alkoxy chain is required for these oligothiophenes to form thermotropic liquid-crystalline phases. In general, this group of molecules displayed a broad temperature range of highly ordered smectic phase, which will be confirmed in detail in the following section to be smectic E (SmE), rich crystalline polymorphism and mostly a nematic (N) phase (Table 1, see the Supporting Information for the DSC thermograms). Their mesogenic clear points decreased with an extended alkoxy tail from a decyloxy to an octadecyloxy group. Furthermore, those compounds with an alkoxy tail with ten to fourteen methylene

Table 1. Phase transition temperatures and enthalpies for all compounds **2–16**.<sup>[a]</sup>

	Transition temperature [ $^\circ\text{C}$ ] (enthalpies [ $\text{J g}^{-1}$ ])							
	Heating ( $10^\circ\text{C min}^{-1}$ )				Cooling ( $10^\circ\text{C min}^{-1}$ )			
<b>2</b>	65.9 (84.5)							
	K→I							
<b>3</b>	113.9 (70.9)				77.7 (–11.1)			
	K→I				I→K			
<b>4</b>	97.9 (0.63)	137.5 (26.9)	178.8 (39.4)	194.6 (1.06)	193.6 (–1.37)	175.9 (–38.5)	137.3 (–0.80)	95.0 (–14.4)
	K2→K1	K1→SmE	SmE→N	N→I	I→N	N→SmE	SmE→K1	K1→K2
<b>5</b>	95.2 (1.06)	130.0 (11.3)	176.9 (22.5)	183.6 (0.62)	182.3 (–0.62)	174.1 (–22.8)	130.5 (–0.42)	75.1 (–2.98)
	K2→K1	K1→SmE	SmE→N	N→I	I→N	N→SmE	SmE→K1	K1→K2
<b>6</b>	93.6 (0.82)	131.3 (37.7)	174.9 (31.4)	179.2 (0.84)	177.1 (–1.37)	170.4 (–32.6)	131.1 (–0.50)	66.7 (–8.61)
	K2→K1	K1→SmE	SmE→N	N→I	I→N	N→SmE	SmE→K1	K1→K2
<b>7</b>	91.3 (1.18)	125.1 (27.4)	137.3 (0.15)	172.0 (28.2)	173 <sup>[b]</sup>	171 <sup>[b]</sup>	168.9 (–28.4)	133.4 (–0.35)
	K3→K2	K2→K1	K1→SmE	SmE→N	N→I	I→N	N→SmE	SmE→K1
<b>8</b>	92.4 (1.23)	121.7 (18.0)	141.2 (0.26)	171.0 (38.2)	167.9 (–37.3)	136.4 (–0.45)	67.9 (–17.6)	
	K3→K2	K2→K1	K1→SmE	SmE→I	N→SmE	SmE→K1	K1→K2	
<b>9</b>	95.7 (62.4)				72.8 (–61.7)			
	K→I				I→K			
<b>10</b>	118.4 (36.1)	150.5 (7.16)	153 <sup>[b]</sup>		153 <sup>[b]</sup>	148.5 (–7.12)	128 <sup>[b]</sup>	97.5 (–32.7)
	K→SmA	SmA→N	N→I		I→N	N→SmA	SmA→SmC	SmC→K
<b>11</b>	123.5 (2.81)	147.3 (12.5)	188 <sup>[b]</sup>	216.7 (6.65)	215.1 (–6.68)	188 <sup>[b]</sup>	144.3 (–12.2)	106 <sup>[b]</sup>
	S2→S1	S1→SmC	SmC→SmA	SmA→I	I→SmA	SmA→SmC	SmC→S1	S1→S2
<b>12</b>	186.4 (4.24)	240.0 (25.5)	289.1 (0.40)	298.0 (9.56)	296.2 (–8.33)	287.8 (–0.10)	237.0 (–24.8)	162.2 (–6.03)
	S2→S1	S1→SmC	SmC→SmA	SmA→I	I→SmA	SmA→SmC	SmC→S1	S1→S2
<b>13</b>	28.3 (22.5)	109.8 (51.6)			54.1 (–40.4)	17.6 (–21.9)		
	K2→K1	K1→I			I→K1	K1→K2		
<b>14</b>	135.5 (50.6)				128.2 (–6.89)	117.0 (–40.9)		
	K→I				I→SmA	SmA→K		
<b>15</b>	190.4 (45.5)	213.0 (7.57)			211.1 (–7.57)	180 <sup>[b]</sup>	157.1 (–40.3)	
	K→SmA	SmA→I			I→SmA	SmA→SmC	SmC→K	
<b>16</b>	190 <sup>[b]</sup>	247.9 (39.5)	270.7 (1.26)	289.5 (9.49)	286.9 (–9.39)	268.7 (–1.35)	240.3 (–38.0)	120 <sup>[b]</sup>
	S2→S1	S1→SmC	SmC→SmA	SmA→I	I→SmA	SmA→SmC	SmC→S1	S1→S2

[a] The transition enthalpies [ $\text{J g}^{-1}$ ] are given in parentheses; a positive value stands for endothermic, a negative value means exothermic. Data from the second heating and first cooling cycles; I stands for isotropic phase; N for nematic; SmA, SmC, and SmE for smectic A, C and highly ordered smectic E phase, respectively; S1 and S2 represents the high and low temperature layered condensed phase, respectively. K stands for crystal, K1 and K2 for the high and low melting point crystalline polymorph, respectively. [b] These thermal transition data were obtained from POM observations without detectable transition peaks or enthalpy changes on the DSC curves.

units in this series (**4–6**) exhibited enantiotropic nematic phases of decreasing temperature range, their nematic phases were confirmed both by their small (less than  $1.5 \text{ J g}^{-1}$ ) transition enthalpies and the typical schlieren or thread textures, as shown in Figure 1 a. Despite an undetectable transition in the DSC trace, a narrow schlieren texture of the nematic phase was observed under POM for the hexadecyloxy-substituted oligomer **7**. On the other hand, the longest octadecyloxy-substituted oligomer **8** possessed only an ordered SmE phase with the brightest natural mosaic texture generated directly from the isotropic black field (Figure 1 b).<sup>[21]</sup> Less-bright mosaic textures, as representatively shown in Figure 1 c, were all observed in the SmE phases of compounds **4–7** of this series and were transformed from

the preceding N phase schlieren textures. Upon cooling to the crystalline phase markedly dimmed mosaic textures with many disclination black lines were usually obtained, as shown in Figure 1 d for **8** as an example. Such a desirable phase sequence is reminiscent of the similar phase behavior exhibited by 5,5''-bis(5-alkyl-2-thienylethynyl)-2,2':5',2''-terthiophene. The gradual increase in order and the slow transitions between the phases were demonstrated to be a useful characteristic for obtaining a large-area liquid-crystal monodomain.<sup>[9b,c]</sup>

For the double end-capped series,  $\text{C}_{10}\text{O-Ar-OT}(n)\text{-R}$  ( $\text{R} = \text{Ph-SC}_6$  and  $\text{Ph-SO}_2\text{C}_6$ ;  $n = 1, 2, 3, 4$ ), apart from the one-thiophene-containing derivatives **9** and **13**, exhibited various smectic A (SmA) and smectic C (SmC) phases, crystal polymorphs, and low-temperature solid-phase transitions. Interestingly, for those three- or four-thiophene-containing oligomers, some special low-temperature layered condensed phases were observed. This sub-group provided a platform to explore the influences of the rigid oligothiophene conjugation length and the polarity of linking end substituents. For oligomers with a nonpolar alkylsulfanyl terminal group (i.e., **9–12**), both the crystal melting point and mesogenic clear point (cp) increased significantly with increasing oligothiophene conjugation length. The one-thiophene-ring derivative **9** only showed a sharp melting point. On the other hand, the bithiophene derivative **10** exhibited enantiotropic nematic and SmA phases with typical schlieren and focal conic fan textures, respectively, and also a monotropic SmC phase with schlieren and/or paramorphic broken focal conic fan textures. This SmC phase could be observed by POM on the cooling cycle despite lacking a detectable transition peak in the DSC curve due to the very small enthalpy change during the SmA–SmC transition. With extending the oligothiophene core to three or four thiophene rings as **11** and **12**, broad enantiotropic SmA and SmC phases with typical textures, as representatively shown in Figure 1 e and f were observed. When the

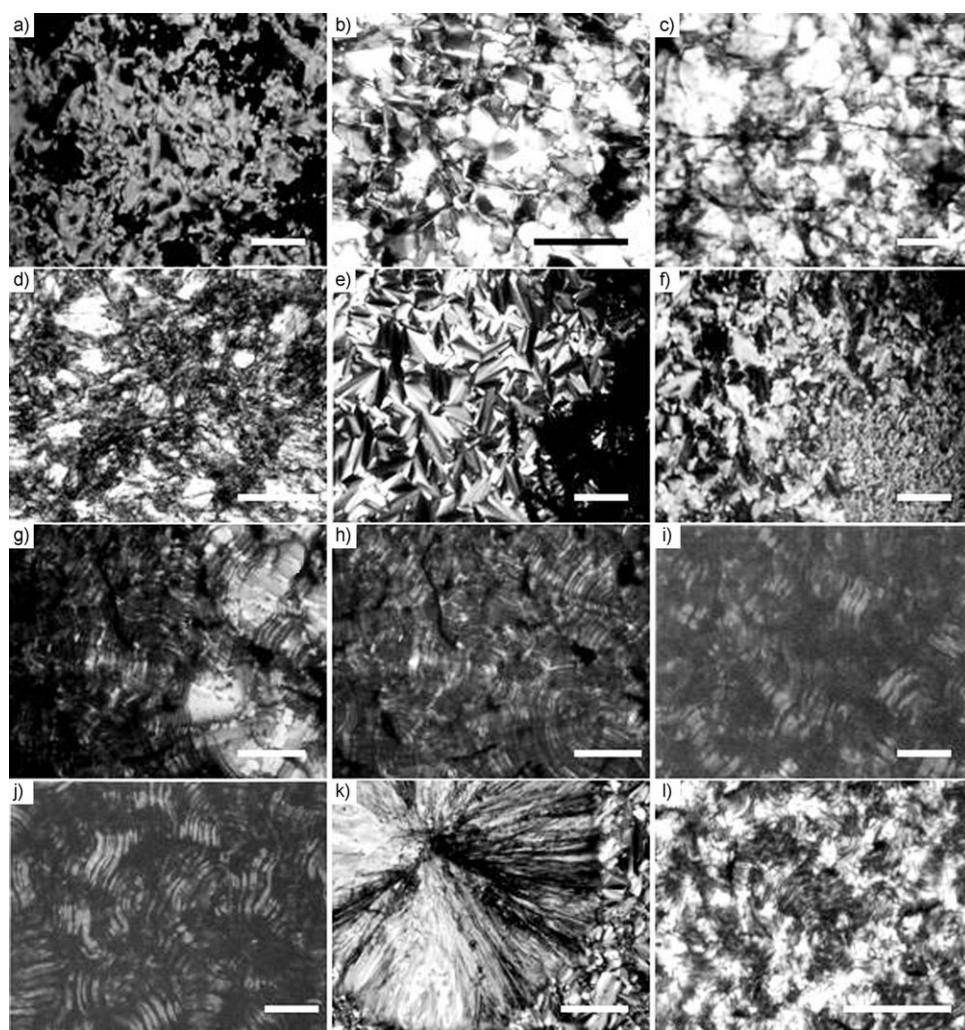


Figure 1. Representative POM textures with crossed polarizers of a) **4**, nematic thread texture at  $185^\circ\text{C}$ ; b) **8**, SmE natural mosaic texture at  $156^\circ\text{C}$ ; c) **7**, SmE mosaic texture at  $160^\circ\text{C}$ ; d) **8**, mosaic texture decorated with black disclination lines of crystalline solid state at  $60^\circ\text{C}$ ; e) **12**, cooling to  $284^\circ\text{C}$ , SmA, focal conic fan and homeotropic texture; f) **12**, cooling to  $270^\circ\text{C}$ , SmC, paramorphic broken focal conic fan and schlieren texture; g) **12**, cooling to  $238^\circ\text{C}$ , transition from SmC broken focal conic fan to S1 striated texture; h) **12**, cooling to  $230^\circ\text{C}$ , striated texture; i) **16**, cooling to  $150^\circ\text{C}$ , thick striped texture; j) **16**, cooling to room temperature  $25^\circ\text{C}$ , thick striped texture with separation lines; k) **14**, cooling to  $116^\circ\text{C}$ , crystalline spherulite growing from the SmA phase; and l) **11**, cooling to  $134^\circ\text{C}$ , fine striated texture. All scale bars correspond to  $100 \mu\text{m}$ . (This figure is provided in color in the Supporting Information.)

polarity of the terminal group increased by oxidizing the alkylsulfanyl to an alkylsulfonyl group, the alkylsulfonylphenyl-substituted oligomers **13–16** showed significantly increased melting points and diminished mesogenic temperature intervals than their corresponding alkylsulfanyl counterparts. Strikingly, for oligomers with four thiophene rings, such as **12** and **16**, striped textures with equidistant lines (Figure 1g–j) characteristic of helical structures were unexpectedly observed under POM in the low-temperature phase in sharp contrast to the typical spherulite or mosaic crystalline textures of those with one or two thiophene rings, such as in **9**, **10**, **13**, and **14** (Figure 1k). In addition, the three-thiophene-ring oligomer with an alkylsulfanylphenyl terminal group (**11**) showed a fine striated texture upon cooling from its preceding fluidic smectic phase (Figure 1l), but not for the corresponding alkylsulfonylphenyl-substituted oligomer **15**. In general, the striped textures appeared on cooling from the preceding SmC broken focal conic fan textures at temperatures well matched with those peak temperatures extracted from DSC measurements. Such textures could reversibly change back into an SmC phase upon heating for **11**, **12**, and **16**, showing a distinct transition between the SmC and condensed phase S1 on both cooling and heating cycles, whereas the striated lines became gradually dimmer when cooling from the SmC phase and then got brighter upon heating again for **11** and **12**. The pitch, determined as the distance between two adjacent dark lines,<sup>[21b]</sup> was almost unchanged with temperature for **11**: ( $4.9 \pm 0.47$ )  $\mu\text{m}$  at  $140^\circ\text{C}$  and ( $4.8 \pm 0.34$ )  $\mu\text{m}$  at  $40^\circ\text{C}$ . The pitch reduced slightly with decreased temperature for **12**, for instance, ( $6.8 \pm 1.2$ )  $\mu\text{m}$  at  $195^\circ\text{C}$  and ( $6.0 \pm 0.8$ )  $\mu\text{m}$  at  $30^\circ\text{C}$ . Alternatively, for the alkylsulfonylphenyl-substituted oligomer **16**, the thick striped texture became clearer and clearer upon cooling with some clear separation lines appearing upon cooling to the transition temperature ( $120^\circ\text{C}$ ) for the S1 into S2 phase (Figure 1j) and coagulated again into a continuous striped texture upon heating above  $190^\circ\text{C}$ . Despite these remarkable visual changes, the measured pitch was almost unchanged with temperature, approximately ( $22.5 \pm 1.9$ )  $\mu\text{m}$ , but showed observable expansion and coalition when closely approaching the transition temperature into SmC broken fan texture upon heating. The distinct striated textures or striped patterns are reminiscent of the classical textures for twisted smectic phases from chiral compounds<sup>[21b,22]</sup> or from achiral bent-core molecules.<sup>[16,23]</sup> This unanticipated superstructure was attributed to the helical supramolecular stacking of the asymmetric end-capped extended conjugating oligothiophenes due to steric packing effects or to bent-core conformational chirality under constraint conditions, which will be discussed in detail in the next section combined with XRD characterization and optical spectroscopic investigations. For comparison and clarity, the phase polymorphic transitions are summarized in Table 1 and phase thermograms and 28 supplementary POM plates are provided in the Supporting Information.

**Supramolecular structure in the mesophases:** To investigate the packing structures of the mesophases of these two arylene-capped oligothiophene series, variable-temperature XRD measurements were carried out and compared with the thermal analysis results from DSC and POM.

For the double end-capped series, the XRD-measured lamellar spacing ( $d$ ) showed comparable dimensions with the corresponding optimized molecular contour lengths in their SmA phases and significantly reduced values in the SmC phases, which indicates an obvious tilting arrangement. For instance, on cooling from the isotropic state to  $195^\circ\text{C}$ , the XRD pattern of compound **11** showed a sharp peak in the small-angle region (SAR,  $2\theta < 10^\circ$ ) with a layer spacing of  $39.2 \text{ \AA}$ , which is in good agreement with the molecular length of  $38.4 \text{ \AA}$ . The XRD pattern also showed a diffuse peak in the wide-angle region (WAR), indicative of a liquid-like in-plane order, which is typical for the SmA phase. Further cooling to  $160^\circ\text{C}$ , the XRD pattern possessed similar features with reduced layer spacing ( $d = 36.8 \text{ \AA}$ ), together with the DSC analysis and POM observation, the SmC phase could be assigned unambiguously, and the tilting angle related to the layer normal was around  $17^\circ$  based on the optimized molecular length calculation. Upon further cooling, a sharp reflection together with its high orders up to the fourth order in the SAR and diffuse scatterings in the WAR were observed (see the Supporting Information), indicating the formation of a unique well-defined lamellar structure. The  $d$  spacing further decreased to  $33.4 \text{ \AA}$  in the  $135^\circ\text{C}$  high-temperature condensed phase S1 and  $30.2 \text{ \AA}$  in the  $50^\circ\text{C}$  lower-temperature phase S2. These phase-transition sequences were commonly observed for the double end-capped oligomers containing three or four thiophene rings, as representatively listed in Table 2 for compounds **11** and

Table 2. The lattice spacings at various temperatures of representative double end-capped oligothiophenes compared with their optimized molecular contour lengths.

	<b>11</b>	<b>16</b>	Phase assigned
$d$ [ $\text{\AA}$ ]/ $T$ [ $^\circ\text{C}$ ]	39.2/195	45.5/285	SmA
	36.8/160	43.3/265	SmC
	33.4/135	39.8/200	S1
	30.2/50	37.8/50	S2
Molecular length <sup>[a]</sup> [ $\text{\AA}$ ]	38.4	44.6	–

[a] Measured in optimized molecular geometry by MM+ calculations in HyperChem 7.5.

**16.** Further molecular tilting or conformational twisting and alkyl chain interdigitation should account for these ever-shortened layer spacings. The clear lamellar structure and equidistant striped POM textures are reminiscent of those features exhibited by polar SmCP or B2 phases of bent-core or banana-shaped molecules.<sup>[16,23]</sup>

For the single end-capped series, compound **4**, for instance, after annealing at the isotropic temperature of  $195^\circ\text{C}$  for five minutes to eliminate the effect of thermal history, formed an imperfect crystalline phase upon rapid

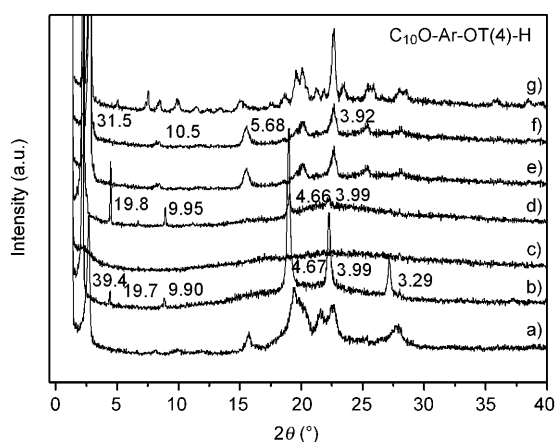


Figure 2. Variable temperature XRD patterns of **4** a) cooling to 50°C, b) heating to 160°C, c) heating to 190°C, d) cooling to 170°C, e) cooling to 110°C, f) cooling to 50°C, and g) cooling to room temperature (23°C).

cooling down to 50°C, as shown in Figure 2 (curve a). Then upon heating to the mesophase temperature of 160°C (Figure 2, curve b), sharp higher-order reflections were observed in the SAR and several marked reflection peaks superposed on the broad band in the WAR consistently indicated the formation of a highly ordered smectic phase.<sup>[3f,9b,c,24,25]</sup> All the peaks could be indexed with a centered rectangular smectic E (SmE) phase as 39.4 (001), 19.72 (002), 9.90 (004), 4.67 (110), 3.99 (200), and 3.29 Å (210) with a layer spacing of 39.4 Å. Upon further increasing the temperature to 190°C, it displayed no SAR reflections, but only a diffuse peak in the WAR that confirmed nematic phase formation (Figure 2, curve c). Upon cooling back to 170°C, the SmE phase recovered with relative weak reflections in the WAR (Figure 2, curve d). Further cooling to 110°C led to the formation of a crystalline phase with a layer spacing of 33.2 Å (Figure 2, curve e) and then cooling to 50°C resulted in another crystalline phase with a slightly reduced spacing of 31.5 Å (Figure 2, curve f). A complex crystalline polymorphism was achieved after the sample was further cooled to 23°C and left to stand overnight with two main lattice spacings of 35.0 and 31.3 Å (see Figure 2, curve g and also the Supporting Information).

Other compounds in this series exhibited quite similar XRD patterns to those of compound **4**, along with even stronger crystallization inhibition upon cooling from the melt. The  $d$  spacing obtained from the ordered smectic phases (160°C) and the crystalline state (50°C) of the whole single end-capped series is plotted versus the methylene number ( $n$ ) of the alkoxy tail in Figure 3. For the ordered smectic phase, the powder XRD patterns usually contain three to four sharp reflections in the SAR corresponding to the one to four orders of the smectic layer period. Among them, the intensity of the third order reflection is significantly diminished or even absent. The smectic period  $d$  grows linearly with the length of the alkoxy tail (Figure 3), according to Equation (1) ( $R=0.996$ ):

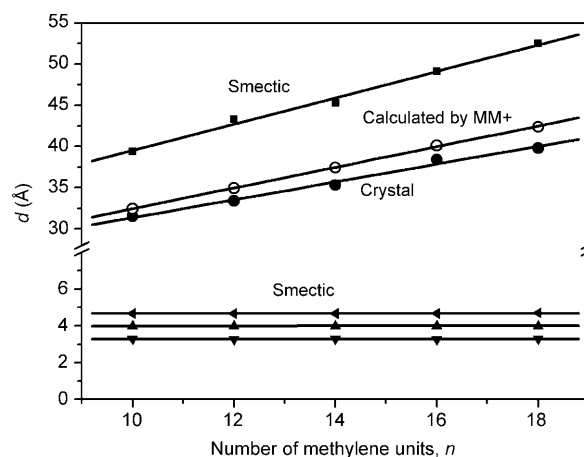


Figure 3. Spacings ( $d$ ) measured by XRD versus the number of methylene units ( $n$ ) of the alkoxy tail in the single end-capped oligothiophenes for the layered crystalline state (●) and for the ordered smectic phase in the SAR (▲) and in the WAR (▼), and the molecular lengths (○) calculated by MM+ simulation for comparison.

$$d [\text{Å}] = (23.52 \pm 1.14) + (1.60 \pm 0.08)n \quad (1)$$

In the WAR, in addition to the diffuse band at  $2\theta$  around  $20^\circ$  related to the molten state of the alkyl chains, all compounds in this series showed three medium to strong intensity peaks (curves b and d in Figure 2 for **4** as an example) with essentially constant spacings as shown in Figure 3 (▲, ▼). These observations are in agreement with those anticipated for an ordered smectic phase with a thickness increasing with the length of the molecules, but lateral packing common to all members.<sup>[25]</sup> According to MM+ geometry optimization, the single end-capped oligothiophenes often adopt an energy-favored stretched conformation as shown, for example, for **6**, in Figure 4a. The calculated  $d$  spacing of the period layers is equal to  $1.2\text{--}1.3 \times$  the molecular length ( $L$ ) simulated by MM+ calculations, an interdigitated antiparallel packing arrangement as shown in Figure 4b was proposed, in which the aromatic–aliphatic diblock molecules oriented alternatively up and down adhered by the  $\pi\text{--}\pi$  interactions between the conjugated oligothiophene part and by the weak van der Waals interactions between alkyl chains forming a two-dimensional ordered lattice structure. Here the dimethyl-substituted phenyl ring may adopt a staggered position for the steric hindrance and contribute to the increased layer spacing. The rotation-limited blade-like molecules adopt a herringbone packing structure, as shown in Figure 4c. Deduced from the  $y$  intercept of  $d(n)$  under the assumption of constant molecular area, which is perfectly legitimate here because they share the same rectangular lateral arrangement independent of the alkoxy chain length, the thickness of the rigid aromatic part  $d_0=23.52$  is in good agreement with the value of 23.42 Å calculated by molecular modeling, assuming the quaterthiophene units are reversely adhered by  $\pi\text{--}\pi$  stacking and the phenyl rings are staggered due to the steric hindrance of the two methyl groups (see the Supporting Information). The

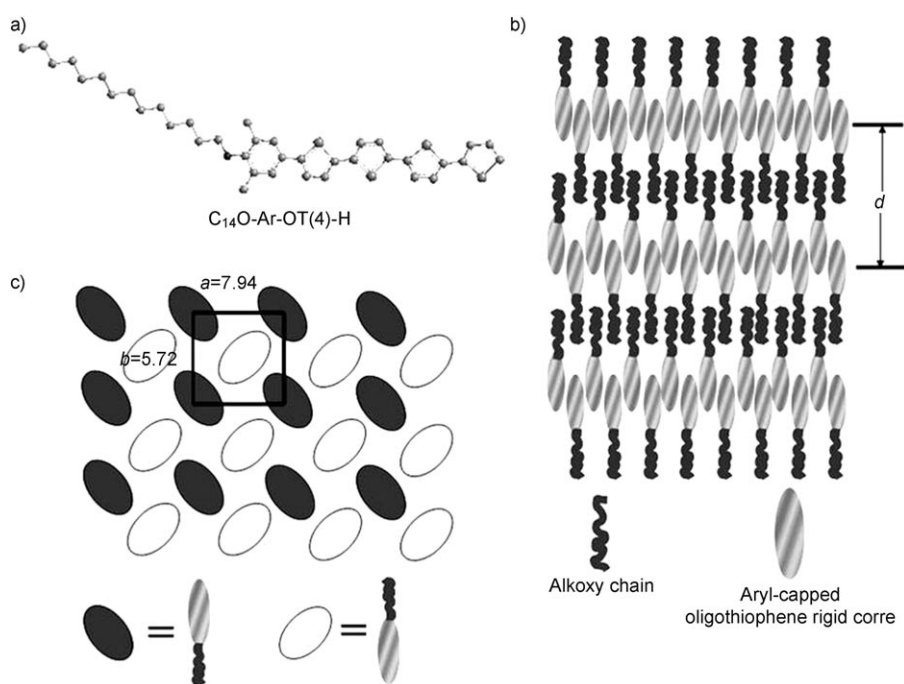


Figure 4. Molecular models of representative compound **6** based on molecular mechanics (HyperChem MM+ Force field) calculations (a) and the proposed packing structure of the single end-capped oligothiophene series in the ordered SmE phase, b) side view and c) top view.

slope of the  $d(n)$  straight line (1.60 Å), which represents the growth rate of the lamellar thickness with the number of methylene groups, is significantly larger than the length of one zigzag in a paraffin chain fully extended interdigitated single layer (1.27 Å) and smaller than the increment (2.54 Å) in an end-to-end double-layer structure, further verified the partially interdigitated arrangement. All XRD data of this series at 160 °C could be accounted for by an orthogonal-centered rectangular lattice, SmE, in which  $a = 7.94$  Å and  $b = 5.72$  Å for compound **6** as an example.

For the crystalline state, aside from some peaks indicative of a three-dimensional crystal lattice, the XRD patterns usually show three reflection peaks with reciprocal spacings in the ratio of 1:2:3 in the SAR, as normally observed with long alkyl-chain derivatives,<sup>[24,25]</sup> revealing that the molecules are arranged in a lamellar fashion. The period of the lamellar structure increases linearly with the number of the methylene units (Figure 3), according to Equation (2) ( $R = 0.995$ ):

$$d [\text{Å}] = (20.56 \pm 0.95) + (1.08 \pm 0.07)n \quad (2)$$

From the  $y$  intercept of  $d(n)$ , the thickness of the rigid aromatic part,  $d_0 = 20.56$ , is in agreement with the value of 20.53 Å calculated by molecular modeling for the aromatic rigid core (see the Supporting Information). Therefore, in the crystalline state, the single end-capped molecules may adopt a fully interdigitated single-layer packing structure thanks to the ever-enhanced interactions among the fully stretched alkyl chains and the steric packing requirement,

whereas in the high-temperature ordered smectic phase the predominant interaction is between the oligothiophene rings. Although we cannot determine the precise crystal structure from the limited efficient peaks due to crystallization inhibition, it can be deduced from the slope of 1.08 Å that the molecules only need to slightly tilt away from the rigid core parallel to layer normal arrangement by an angle of less than 10°; the fully stretched alkyl chain has an angle of approximately 155° with the rigid part according to results of the MM+ optimization (see the Supporting Information).

**CD/UV-visible spectroscopic investigations and supramolecular chirality:** For those double end-capped oligothiophenes exhibiting unique striped POM textures at temperatures lower

than fluid smectic phases, we performed circular dichroism (CD) measurements and spectroscopic investigations to explore further their packing structure and supramolecular chirality. Figure 5a shows that the CD and UV/Vis absorption spectra of solid films of **12**, which contains the nonpolar alkylsulfanylphenyl terminal group, have striped POM textures. Interestingly, strong CD signals exhibiting remarkable bisignate Cotton effects with the crossing wavelength basically coinciding with the absorption maximum of UV/Vis spectra of the films were observed, which suggests the formation of a well-defined helical stacking sequence and the existence of supramolecular chirality. The three-thiophene-containing analogue **11**, which showed a fine striated texture, also exhibited a distinct CD signal in a similar fashion (see the Supporting Information). Moreover, solid films of **16**, which has a polar alkylsulfanylphenyl terminal group, showed a thick striped pattern and exhibited strong CD signals with a different, almost unimodal, Cotton effect essentially consistent with the UV/Vis absorption spectra of the films, as shown in Figure 5b. Such unimodal CD response is reminiscent of that of a helical structure formed by banana-shaped molecules.<sup>[26]</sup> On the other hand, compound **15** and other shorter oligothiophene analogues showed no significant optical activity. For those samples showing optical activity, we noted that the sign of the CD signals altered from overall positive (right-handedness,  $P$ , black curve) to negative (left-handedness,  $M$ , grey curve) on different parts of the same sample or upon different sample preparations, although the spectral wavelengths scarcely changed, as shown in Figure 5a and b. This suggests that the observed CD

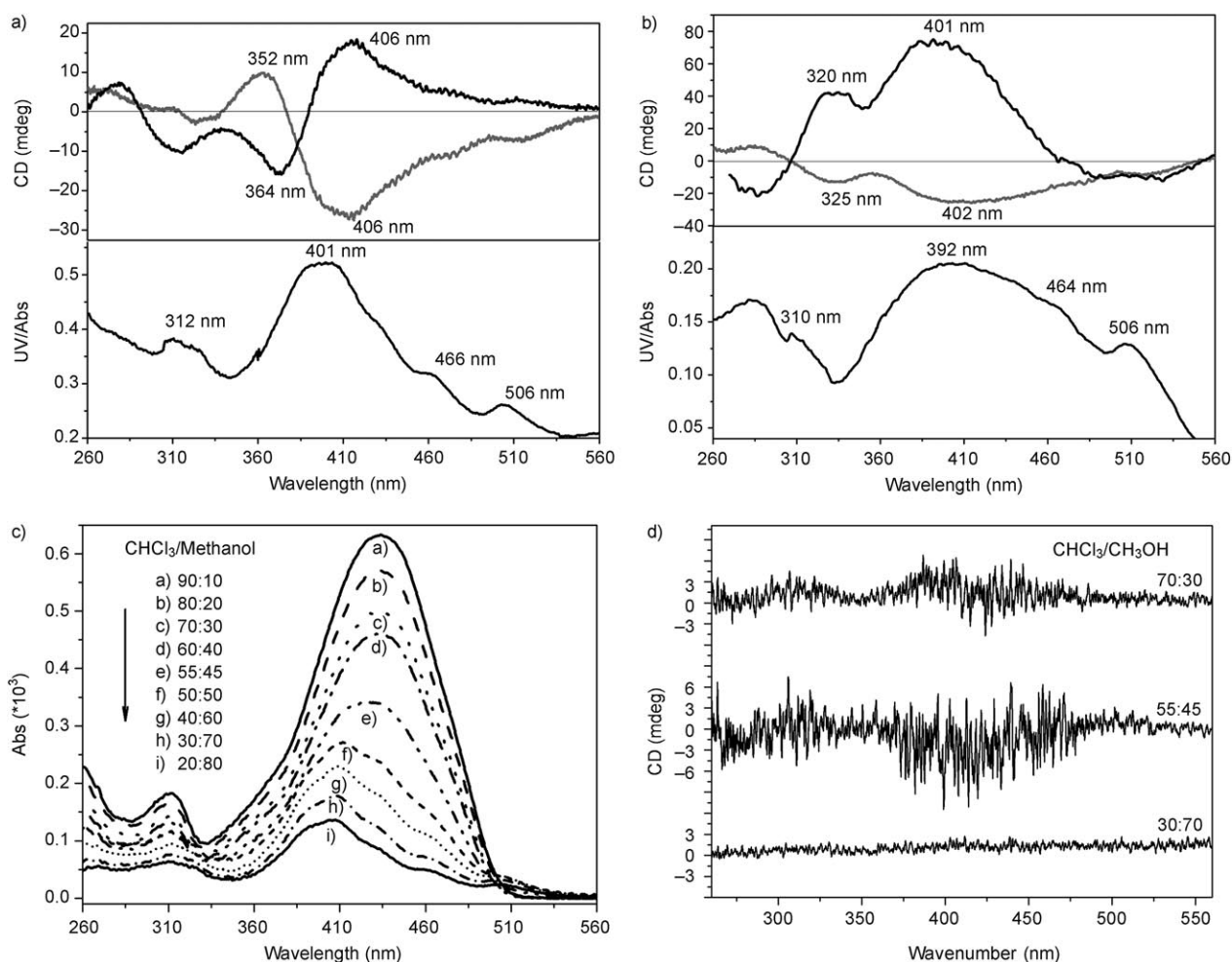


Figure 5. CD and UV/Vis spectra of solid films at room temperature of a) **12**; b) **16**, the overall positive (black) and negative (grey) curves were measured on different locations of the same film; and c) UV/Vis absorption spectra and d) CD spectra of compound **12** in chloroform/methanol mixed at different ratios.

effect resulted from an unbalanced formation of the two domains of opposite chirality. The right- and left-handed helices occurred randomly, which is similar to those observed previously from achiral bent-core molecules,<sup>[16b,26,27]</sup> coordination polymer crystals,<sup>[17]</sup> and supramolecular helical assemblies from achiral amphiphiles in an air/water interface.<sup>[18]</sup> Furthermore, to shed light on the packing behavior in the aggregated state, the optical properties of **12** were investigated by changing from the molecularly dissolved state in chloroform to a gradually aggregated state in poorly dissolved solvent, that is, methanol as shown in Figure 5c. With an increase in the volume ratio of methanol, the UV/Vis absorption spectra from the molecularly dissolved state, with a principal broad absorption band maximum at  $\lambda = 433$  nm in  $\text{CHCl}_3$ , blueshifted to around 410 nm, particularly when the methanol volume ratio was more than 45%. A sharp transition of the spectral shape with a distinct blueshift and the appearance of new fine vibronic shoulders at  $\lambda = 460$  and 505 nm strongly support the formation of aggregates. The large blueshift in the UV/Vis spectrum for aggregate formation suggests that the supramolecular organization formed

in this case is tightly packed, which results in a strong excitonic coupling similar to those of oligothiophenes with oligo(ethyleneoxide) tails<sup>[19,22b]</sup> that have been demonstrated to arrange in an H-type aggregate.<sup>[29]</sup> The UV/Vis spectra of the aggregated form of **12** in solution is quite similar to that of its thin solid film; nevertheless, the CD measurements did not show any distinct signals (Figure 5d and for **16** in solution see the Supporting Information), which suggests that either the aggregate formed is achiral or the chiral aggregates in solution are racemic with which no CD response is observed. Furthermore, the CD signals of the thin films result from not only the aggregation packing, but also the constraint in the solid-state phase, which plays a key role for the generation of optical activity.

It has been proposed that  $\pi$ -stacking interactions play a central role in the supramolecular assembly of poly-/oligothiophene derivatives into an aggregation in solution. Meanwhile, the interplay between the conjugated molecules and solvent molecules is also of primary importance.<sup>[30–32]</sup> In the solid state, interactions with solvent molecules are absent and the driving forces for the supramolecular organization

are the intermolecular interactions between the conjugated species and the substrate surface, the intrinsic constraints, and the noncovalent interactions, such as  $\pi$  stacking and van der Waals interactions, which are crucial in determining thin-film properties.<sup>[19,33]</sup> Determination of the origin of the helicity and chirality from achiral molecules has been an intriguingly important research topic in the liquid-crystal field.<sup>[15,16,26,27]</sup> Recently, the achiral (without the asymmetric carbon) banana-shaped bent-core molecules have been extensively studied because they exhibit various kinds of unusual smectic phases (banana phases) with chiral and/or helical smectic structures.<sup>[16b,26,34]</sup> The twisting conformation, the tilting of molecules in a smectic layer, and the escape from the macroscopic polar order within a layer have been considered as origins of the chirality or helicity and the mechanism of spontaneous desymmetrization in such smectic mesophases from banana-shaped achiral molecules.<sup>[16b,26,34]</sup> In poly-/oligothiophenes, each C–C bond is a potential center of chirality by atropisomerism depending on various intrinsic and extrinsic factors, such as a subtle change in the solvent, has significantly altered or inverted the chirality of chiral aggregates thus formed in solution.<sup>[30,35]</sup> For the asymmetrically double end-capped oligothiophenes, in view of the distinct striped texture, the strong CD effects and the well-defined smectic layer structure with marked shortened spacing and diffuse WAR scatterings from XRD analyses, a helical packing model comparable to that from banana-shaped achiral molecules<sup>[16b,23]</sup> is proposed, as illustrated in Figure 6. The preference of the bent-core banana-shaped conformation and the helix formation can be triggered by lowering of the temperature and the constraint thus produced in the solid phase, which results in the chiral symmetrical breaking and optical activity in the solid films, as reversibly demonstrated that it could not realize in the ordered fluidic mesophases.<sup>[36]</sup> The phase behavior exhibited

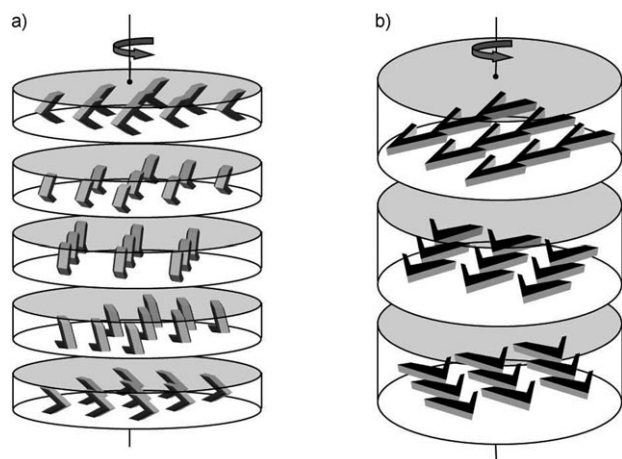


Figure 6. Schematic illustrations of the molecular packing in the banana-shaped conformation and the smectic-like layer structures. a) The helical structure along the layer normal in the nonpolar alkylsulfanylphenyl end-capped oligothiophene derivatives **11** and **12**, and b) the helical axis lying in the layer for the polar alkylsulfanylphenyl end-capped oligothiophene derivative **16**, similar to the TGB phase.

by the simple hockey-shaped molecules<sup>[27,37,38]</sup> provides us strong hints at the least deviation from the conventional straight-core mesogen geometry required to form a banana-shaped molecule, as well as the fact that the longer alkyl chain can help to realize the desymmetric superstructure organization and thus exhibit supramolecular chirality. The asymmetric structures with donor and acceptor substituents in the double end-capped oligothiophenes thus possessing an intrinsic dipole can provide a polar order. Furthermore, the *cis* conformation of the double end-capped quaterthiophene derivatives **16** (pseudo-banana shaped) has a very similar total energy as the *trans* conformation (*Z* shaped) as optimized by MM+ (see the Supporting Information). With the hexyl and decyl alkyl chain on either end, the formation of a true banana-shaped molecule with twisting conformation leading to a tilted chiral molecular arrangement to escape from spontaneous polarization should be reasonable. Two types of helical structure with remarkably different pitches and brightnesses were observed as described above. For the nonpolar alkylsulfanyl end-capped **11** and **12**, the striated patterns are superimposed on the fan-shaped textures. It is believed that the  $\pi$ – $\pi$  stacking of the aromatic rigid core and the cooperative van der Waals interactions among alkyl chains provide the driving force for the association of somewhat bent molecules under confined conditions. In addition, the two methyl groups substituted at the phenyl ring together with steric-packing requirements may arouse the twisting and thus the helical superstructure formation in which the helical axis is perpendicular to the layer, similar to the chiral SmC\* phase as shown in Figure 6a. On the other hand, the polar alkylsulfanyl end-capped **16** showing a much larger pitch exhibited a dark field under crossed polarizers for a very short time, which implies that a transient homeotropic state occurs before the arrival of the thick striped pattern texture. Therefore, the helical twisting of molecules takes place along the layer and the helical axis lies in the layer similar to that observed in the twisted grain boundary (TGB) phase as shown in Figure 6b. The polar order induced by the polar alkylsulfanyl group clearly provides the driving force for twisting to escape from macroscopic polarization. The supramolecular chirality produced by the steric interfacial packing of achiral amphiphilic molecules provided a simple two-dimensional model for our system.<sup>[18]</sup>

Some further work such as electro-optic experiments may be needed to gain a detailed understanding of the supramolecular chirality exhibited by the alkyl-substituted, almost-straight aromatic core achiral molecules; however, we can currently propose that the chirality achieved in this system originates from the supramolecular organization of the uniquely designed asymmetric molecules in helical stacking structures of somewhat twisted conformers. These asymmetrically double end-capped oligothiophenes also represent the first achiral, almost-straight, aromatic-core-based mesogens that exhibit supramolecular chirality.

**FET properties:** To explore the potential applications of the single end-capped oligothiophenes  $C_m$ -Ar-OT(4)-H with a

highly ordered smectic phase in OFET, top-contact OFETs using **4** as a semiconductor layer were fabricated on plain and octyltrichlorosilane (OTS)-treated (nonmodified or octylsilane-modified) SiO<sub>2</sub>/Si substrates by high-vacuum evaporation according to a published procedure.<sup>[39]</sup> Different substrate deposition temperatures ( $T_d$ ) were investigated to evaluate the effect of mesophases on the OFET performances. The electrical measurements were carried out at room temperature under ambient conditions. Compound **4** was found to exhibit typical p-type organic semiconductor characteristics, as shown in Figure 7. The hole mobilities were

respectively,  $\mu$  is the field-effect mobility,  $C_i$  is the capacitance per unit area of the SiO<sub>2</sub> layer, and  $V_G$  and  $V_T$  are the gate voltage and threshold voltage, respectively. In our case, the channel length is 45  $\mu$ m and the channel width is 2.5 mm.

Compound **4** deposited at  $T_d=25^\circ\text{C}$  on plain and OTS-treated substrates showed hole carrier mobilities of  $4.6 \times 10^{-3}$  and  $8 \times 10^{-3} \text{ cm}^2 \text{ V}^{-1} \text{ s}^{-1}$ , respectively, and on/off current ratios of about  $10^5$ . When the substrate temperature was increased to  $T_d=140^\circ\text{C}$  during film deposition, the hole mobilities on plain and OTS-treated substrates improved and reached 0.052 and  $0.07 \text{ cm}^2 \text{ V}^{-1} \text{ s}^{-1}$ , respectively. The on/off current ratios also slightly increased to  $5 \times 10^5$ . Both the hole mobilities and on/off current ratios are comparable to the highest values reported for the series of symmetrical hexyl-phenyl double end-capped phenylene-thiophene co-oligomers by Marks and co-workers.<sup>[11]</sup> This strong dependence of the mobility of **4** on the substrate temperature during evaporation is in good agreement with the DSC result showing the formation of a highly ordered smectic E phase above  $137.5^\circ\text{C}$ .

As further evidenced by XRD analysis, the molecules in the vacuum-deposited films at both 25 and  $140^\circ\text{C}$  adopt an organization in which the  $\pi$ - $\pi$  stacking direction is parallel to the substrate surface. This kind of organization is known to be favorable for high mobility in OFETs.<sup>[8,9]</sup> In addition, Figure 8 shows some difference in the XRD patterns for the films deposited at different temperatures. The  $\omega/2\theta$  scan of the film of **4** deposited at a substrate temperature of  $140^\circ\text{C}$  shows a diffraction peak at  $2.8^\circ$  and a second order line at  $5.6^\circ$ , corresponding to a repeat distance (periodicity) of 3.20 nm. This  $d$ -spacing value suggested that the molecules are almost perpendicular to the substrate. The curve also shows nice thickness oscillations, indicating that the film is quite smooth. The periodicity of the fringes suggests that the molecules self-organized into ten repeats of vertically aligned chains at this deposition temperature. For the film deposited at  $25^\circ\text{C}$ , XRD measurements also showed two diffraction peaks at  $2.83$  and  $5.65^\circ$ , respectively, corresponding to a slightly shorter periodicity of  $\approx 3.15$  nm. However, the curve does not display the thickness fringes. This suggests that the molecules are again predominantly stacked perpendicular to the surface, but the stacking is disordered. This explains the strong diffraction peak, but absence of periodic fringes and thus relatively lower hole mobility.

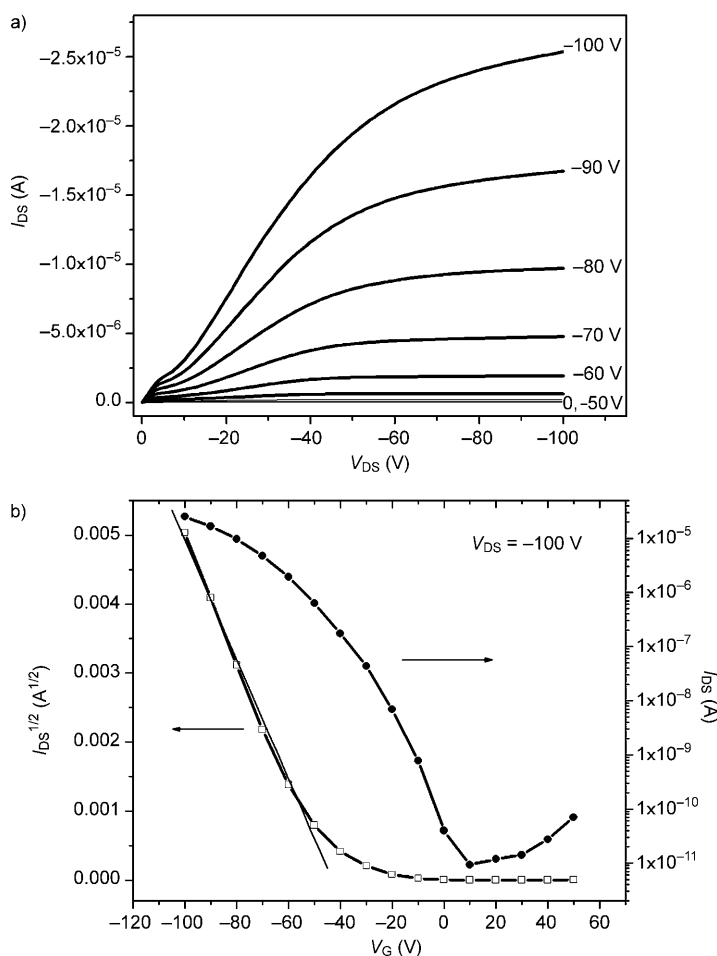


Figure 7. a) Source-drain current ( $I_{DS}$ ) versus source-drain voltage ( $V_{DS}$ ) at various gate voltages ( $V_G$ ) of **4** based top-contact OFETs deposited at  $140^\circ\text{C}$  on plain SiO<sub>2</sub>/Si substrates. b) The transfer characteristics in the saturation regime at a constant source-drain voltage of  $-100$  V.

calculated in the saturation regime at  $V_{DS} = -100$  V by using Equation (3):

$$I_{DS} = (W/2L)\mu C_i (V_G - V_T)^2 \quad (3)$$

in which  $V_{DS}$  is the source-drain voltage,  $I_{DS}$  is the source-drain current,  $W$  and  $L$  are the channel width and length, re-

## Conclusion

A novel series of asymmetrically end-capped mesogenic oligothiophenes with various oligothiophene core lengths, alkoxy tail lengths, and molecular polarities through introducing an alkylsulfanyl or alkylsulfonyl functionality as the terminal group have been synthesized by palladium-catalyzed Suzuki cross-coupling and/or Kumada addition reactions as key steps. For the single end-capped oligothiophenes,  $C_m\text{O-Ar-OT}(4)\text{-H}$ , in which  $m=10, 12, 14, 16,$  and  $18$  (corresponding to molecules **4-8**, respectively), all oligo-

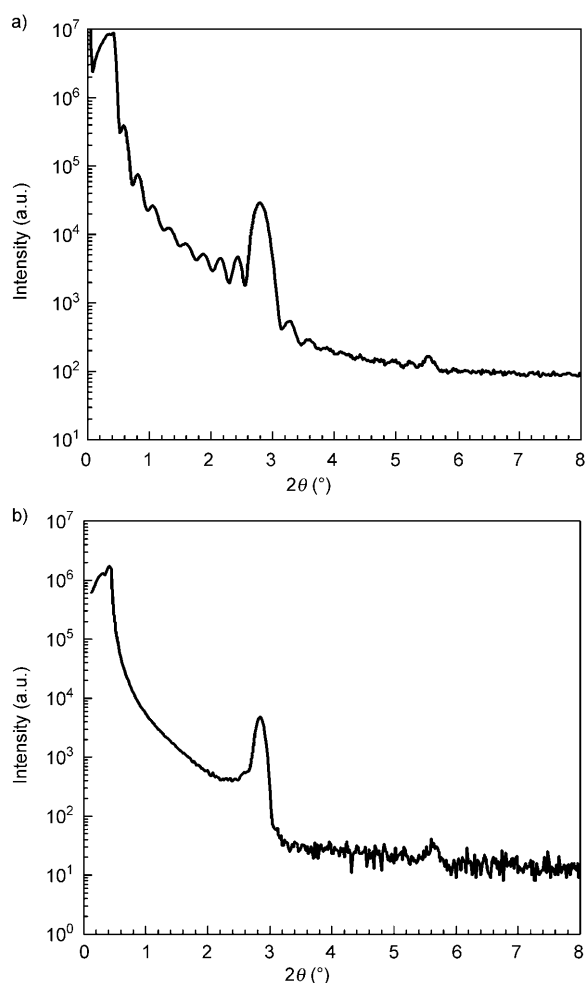


Figure 8. XRD patterns of thin films of **4** vacuum deposited at a) 140 and b) 25 °C.

mers exhibited enantiotropic nematic phases and a broad temperature range of highly ordered SmE phases except for the octadecyloxy-substituted oligomer **8**, which did not show a nematic phase, were confirmed by DSC thermal measurements, POM observations, and XRD analyses. Our initial studies indicated that a high charge mobility of OFET with hole mobility up to  $0.07 \text{ cm}^2 \text{ V}^{-1} \text{ s}^{-1}$  could be achieved with  $\text{C}_{10}\text{O-Ar-OT}(4)\text{-H}$  by taking advantage of its highly ordered SmE liquid-crystalline arrangement.

For the double end-capped series  $\text{C}_{10}\text{O-Ar-OT}(n)\text{-R}$ , in which  $\text{R} = \text{Ph-SC}_6$  or  $\text{Ph-SO}_2\text{C}_6$  and  $n = 1, 2, 3,$  and  $4$  (compound **9–16**), all compounds with two or more thiophene rings were found to exhibit SmA and SmC phases, various crystal polymorphs, and/or unusual low-temperature, layered condensed phases. This series provides a platform to investigate the effects of the rigid oligothiophene conjugation length and the polarity exerted by the end-linking group. For oligomers with an alkylsulfanyl terminal group (compounds **9–12**), both the crystal melting point and mesogenic cp increased significantly with an increase in the oligothiophene conjugation length. Oligomers with a polar alkylsulfanyl terminal group (molecules **13–16**) showed significantly

increased melting points and thus diminished mesogenic temperature intervals than those of their corresponding alkylsulfanyl counterparts. Interestingly, upon cooling from the melted state, crystallization was remarkably inhibited and unusual layered, low-temperature phases formed, particularly for those oligomers with three or four thiophene rings. Two different types of helical structures showing distinct striated textures or regular striped patterns were observed with a pitch of several to tens of micrometers under POM at the low-temperature condensed phases. For nonpolar alkylsulfanyl end-capped **11** and **12**, the striated patterns are superimposed on the fan-shaped textures with a pitch of several micrometers, the helical axis is perpendicular to the layer similar to the chiral SmC\* phase. On the other hand, for the polar alkylsulfanyl end-capped **16**, which shows a thick striped pattern with a much larger pitch of around 22 micrometers, the helical twisting of molecules develops along the layer and the helical axis lies in the layer similar to the TGB phase.

The twisted chiral, smectic phase-like helical structures were further confirmed by XRD analysis and showed well-defined smectic layer structures with markedly shortened layer spacing, and directly evidenced by the distinct CD signals measured from the thin solid films. Furthermore, the optical property investigations of compounds **12** and **16**, by means of changing from the molecularly dissolved state to a gradually aggregated state in mixed solvents, suggested the supramolecular aggregation structures formed with no significant optical activity. So it is believed that the  $\pi$ - $\pi$  stacking of the aromatic rigid core and the cooperative van der Waals interactions among alkyl chains provide the driving force for the association of the somewhat bent molecules under confined conditions in the thin solid films. In addition, the two methyl groups substituted at the phenyl ring together with steric packing requirements may generate the twisting and thus form the helical superstructure. The polar order introduced by the polar alkylsulfanyl group may further drive the in-plane twisting to escape from macroscopic polarization and result in the TGB-like helical structure formation.

This asymmetrically double end-capped oligothiophenes represent the first almost-straight aromatic core achiral molecules that exhibit supramolecular chirality. Our findings could stimulate the search for chiral behavior and further ferroelectricity in a new class of organic semiconducting materials.

## Experimental Section

Detailed synthetic procedures and characterization for all compounds can be found in the Supporting Information. The DSC thermograms were recorded on a Perkin-Elmer Pyris 1 instrument equipped with a cooling accessory and under a nitrogen atmosphere. The temperatures and heat flows were calibrated by employing an indium standard sample. Typically, approximately 4 mg of powdered sample was encapsulated in a sealed aluminum pan with an identical empty pan as the reference. The heating and cooling rate was  $10^\circ\text{C min}^{-1}$ . The phase transitions and

liquid-crystal textures were observed and photographed as melt-pressed preparations sandwiched between a glass slide and a cover glass by using a polarized optical microscope equipped with a Leitz-350 heating stage and a digital CCD camera. The film samples for UV/Vis and CD measurements were melt-pressed and sandwiched between quartz glass. The solutions for CD measurements were prepared from a stock solution of **12** or **16** in chloroform (5 mg/5 mL), then stock solution (0.5 mL) was transferred to a 1 cm quartz cell, with an appropriate volume of methanol and chloroform diluent added according to the predefined ratio so as to keep the total volume (3.0 mL) and the oligomer concentration (0.5 mg/3 mL) constant. For the UV/Vis measurement, the concentration was reduced to 20% with the predefined solvent ratio. The CD signals for the film and the solution were recorded on a JASCO A-810(S) spectropolarimeter with a scanning wavelength range from 190 to 1080 nm. The UV/Vis spectra were performed on a Shimadzu UV-2401 instrument. XRD experiments were performed on a D/max-2550 PC diffractometer with a programmed temperature-controlling oven system using  $\text{Cu}_{\text{K}\alpha}$  (1.5406 Å) as the radiation source with 40 kV, 300 mA power. The film samples cast from a solution in dichloromethane with a thickness of approximately 0.1 mm on clean glass substrate were set on the sample stage and first heated to the isotropic state and then cooled to the liquid-crystal state or the programmed temperatures.

### Acknowledgements

We gratefully acknowledge financial support of this work from the National Natural Science Foundation of China (20874044 and 50273013), the Research Grants Council, Hong Kong (Earmarked Research Grant: HKBU2020/06P) and the Hong Kong Baptist University (FRG/06-07/II-53).

- [1] a) D. Fichou, *J. Mater. Chem.* **2000**, *10*, 571–588; b) G. Barbarella, M. Melucci, G. Sotgiu, *Adv. Mater.* **2005**, *17*, 1581–1593; c) A. R. Murphy, J. M. J. Fréchet, *Chem. Rev.* **2007**, *107*, 1066–1096.
- [2] a) R. Hajlaoui, G. Horowitz, F. Garnier, A. Arce-Bronchet, L. Laiyne, A. E. Kassmi, F. Damanze, F. Konki, *Adv. Mater.* **1997**, *9*, 389–391; b) R. Azumi, G. Götz, P. Bäuerle, *Synth. Met.* **1999**, *101*, 569–572; c) G. Horowitz, M. E. Hajlaoui, R. Hajlaoui, *J. Appl. Phys.* **2000**, *87*, 4456–4463.
- [3] a) F. Garnier, R. Hajlaoui, A. E. Kassmi, G. Horowitz, L. Laigre, W. Porzio, A. Armanini, F. Provasoli, *Chem. Mater.* **1998**, *10*, 3334–3339; b) A. Afzali, T. L. Breen, C. R. Kagan, *Chem. Mater.* **2002**, *14*, 1742–1746; c) M. Halik, H. Klauk, U. Zschieschang, G. Schmid, W. Radlik, S. Ponomarenko, S. Kirchmeyer, W. Weber, *J. Appl. Phys.* **2003**, *93*, 2977–2981; d) S. Ponomarenko, S. Kirchmeyer, *J. Mater. Chem.* **2003**, *13*, 197–202; e) A. R. Murphy, J. M. J. Fréchet, P. Chang, J. Lee, V. Subramanian, *J. Am. Chem. Soc.* **2004**, *126*, 1596–1597; f) M. Funahashi, J. Hanna, *Adv. Mater.* **2005**, *17*, 594–598; g) M. Ashizawa, R. Kato, Y. Takamishi, H. Takezoe, *Chem. Lett.* **2007**, *36*, 708–709; h) S. Ellinger, U. Ziener, U. Thewalt, K. Landfester, M. Möller, *Chem. Mater.* **2007**, *19*, 1070–1075; i) J. Leroy, N. Boucher, S. Sergeev, M. Sferrazza, Y. H. Geerts, *Eur. J. Org. Chem.* **2007**, 1256–1261; j) S. Ellinger, A. Kreyes, U. Ziener, C. Hoffmann-Richter, K. Landfester, M. Möller, *Eur. J. Org. Chem.* **2007**, 5686–5702; k) M. Melucci, L. Favaretto, C. Bettini, M. Gazzano, N. Camaioni, P. Maccagnani, P. Ostojia, M. Monari, G. Barbarella, *Chem. Eur. J.* **2007**, *13*, 10046–10054.
- [4] D. Fichou, C. Ziegler in *Handbook of Oligo- and Polythiophenes*, (Ed.: D. Fichou), Wiley-VCH, Weinheim, **1999**, p. 183.
- [5] M. Funahashi, J. Hanna, *Chem. Phys. Lett.* **2004**, *397*, 319–323.
- [6] Y. Shimizu, K. Oikawa, K. Nakayama, D. Guillon, *J. Mater. Chem.* **2007**, *17*, 4223–4229.
- [7] a) D. Adam, F. Closs, T. Frey, D. Funhoff, D. Haarer, H. Ringsdorf, P. Schuhmacher, K. Siemensmeyer, *Phys. Rev. Lett.* **1993**, *70*, 457–460; b) D. Adam, P. Schuhmacher, J. Simmerer, L. Haussling, K. Siemensmeyer, K. H. Etzbach, H. Ringsdorf, D. Haarer, *Nature* **1994**, *371*, 141–143; c) A. M. van de Craats, J. M. Warman, K. Müllen, Y. Geerts, J. D. Brand, *Adv. Mater.* **1998**, *10*, 36–38; d) V. De Cupere, J. Tant, P. Viville, R. Lazzaroni, W. Osikowicz, W. R. Salaneck, Y. H. Geerts, *Langmuir* **2006**, *22*, 7798–7806; e) T. Yasuda, K. Kishimoto, T. Kato, *Chem. Commun.* **2006**, 3399–3401.
- [8] a) M. Funahashi, J. Hanna, *Phys. Rev. Lett.* **1997**, *78*, 2184–2187; b) M. Funahashi, J. Hanna, *Appl. Phys. Lett.* **1998**, *73*, 3733–3735; c) M. Funahashi, J. Hanna, *Appl. Phys. Lett.* **2000**, *76*, 2574–2576.
- [9] a) P. Vlachos, B. Mansoor, M. P. Aldred, M. O'Neill, S. M. Kelly, *Chem. Commun.* **2005**, 2921–2923; b) O. Lengyel, W. M. Hardeman, H. J. Wondergem, D. M. de Leeuw, A. J. J. M. van Breemen, R. Resel, *Adv. Mater.* **2006**, *18*, 896–899; c) A. J. J. M. van Breemen, P. T. Herwig, C. H. T. Chlon, J. Sweelssen, H. F. M. Schoo, S. Setayesh, W. M. Hardeman, C. A. Martin, D. M. J. de Leeuw, J. P. Valetton, C. W. M. Bastiaansen, D. J. Broer, A. R. Popa-Merticaru, S. C. J. Meskers, *J. Am. Chem. Soc.* **2006**, *128*, 2336–2345.
- [10] H. Maeda, M. Funahashi, J. Hanna, *Mol. Cryst. Liq. Cryst.* **2000**, *346*, 183–192.
- [11] M. Mushrush, A. Facchetti, M. Lefenfeld, H. E. Katz, T. J. Marks, *J. Am. Chem. Soc.* **2003**, *125*, 9414–9423.
- [12] a) S. Hotta, S. A. Lee, *Synth. Met.* **1999**, *101*, 551–552; b) S. A. Lee, Y. Yoshida, M. Fukuyama, S. Hotta, *Synth. Met.* **1999**, *106*, 39–43; c) F. Cicoira, C. Santato, M. Melucci, L. Favaretto, M. Gazzano, M. Muccini, G. Barbarella, *Adv. Mater.* **2006**, *18*, 169–174; d) I. Viola, F. D. Sala, M. Piacenza, L. Favaretto, M. Gazzano, M. Anni, G. Barbarella, R. Cingolani, G. Gigli, *Adv. Mater.* **2007**, *19*, 1597–1602.
- [13] a) H. E. Katz, T. Siegrist, M. Lefenfeld, P. Gopalan, M. Mushrush, B. Ocko, O. Gang, N. Jisrawl, *J. Phys. Chem. B* **2004**, *108*, 8567–8571; b) K. Oikawa, H. Monobe, J. Takahashi, K. Tsuchiya, B. Heinrich, D. Guillon, Y. Shimizu, *Chem. Commun.* **2005**, 5337–5339; c) P. G. A. Janssen, M. Pouderoijen, A. J. J. M. van Breemen, P. T. Herwig, G. Koegelberghs, A. R. Popa-Merticaru, S. C. J. Meskers, J. J. P. Valetton, E. W. Meijer, A. P. H. J. Schenning, *J. Mater. Chem.* **2006**, *16*, 4335–4342; d) M. Funahashi, F. Zhang, N. Tamaoki, *Adv. Mater.* **2007**, *19*, 353–358; e) J. C. Maunoury, J. R. Howse, M. L. Turner, *Adv. Mater.* **2007**, *19*, 805–809; f) A. Sung, M. M. Ling, M. L. Tang, Z. Bao, J. Locklin, *Chem. Mater.* **2007**, *19*, 2342–2351.
- [14] C. D. Dimitrakopoulos, D. J. Mascaró, *IBM J. Res. Dev.* **2001**, *45*, 11–27.
- [15] a) W. J. Lough, I. W. Wainer, *Chirality in Nature and Applied Science*, CRC Press, Oxford **2002**; b) J. J. L. M. Cornelissen, A. E. Rowan, R. J. M. Nolte, N. A. J. M. Sommerdijk, *Chem. Rev.* **2001**, *101*, 4039–4070; c) L. Pérez-García, D. B. Amabilino, *Chem. Soc. Rev.* **2002**, *31*, 342–356; d) M. A. Mateos-Timoneda, M. Crego-Calama, D. N. Reinhoudt, *Chem. Soc. Rev.* **2004**, *33*, 363–372; e) D. R. Link, G. Natale, R. Shao, J. E. MacLennan, N. A. Clark, E. Körblová, D. M. Walba, *Science* **1997**, *278*, 1924–1927; f) G. Heppke, D. Moro, *Science* **1998**, *279*, 1872–1873; g) M. Simonyi, Z. Bikádi, F. Zsila, J. Deli, *Chirality* **2003**, *15*, 680–698; h) M. Suárez, N. Branda, J.-M. Lehn, A. Decian, J. Fischer, *Helv. Chim. Acta* **1998**, *81*, 1–13.
- [16] a) G. Pelzl, S. Diele, W. Weissflog, *Adv. Mater.* **1999**, *11*, 707–724; b) A. Reddy, C. Tschierske, *J. Mater. Chem.* **2006**, *16*, 907–961.
- [17] T. Ezuhara, K. Endo, Y. Aoyama, *J. Am. Chem. Soc.* **1999**, *121*, 3279–3283.
- [18] a) J. Yuan, M. Liu, *J. Am. Chem. Soc.* **2003**, *125*, 5051–5056; b) Z. X. Guo, J. Yuan, Y. Cui, F. Chang, W. H. Sun, M. H. Liu, *Chem. Eur. J.* **2005**, *11*, 4155–4162; c) X. Huang, C. Li, S. Jiang, X. Wang, B. Zhang, M. Liu, *J. Am. Chem. Soc.* **2004**, *126*, 1322–1323; d) P. Z. Guo, L. Zhang, M. H. Liu, *Adv. Mater.* **2006**, *18*, 177–180.
- [19] a) Ph. Leclère, M. Surin, P. Viville, R. Lazzaroni, A. F. M. Kilbinger, O. Henze, W. J. Feast, M. Cavallini, F. Biscarini, A. P. H. J. Schenning, E. W. Meijer, *Chem. Mater.* **2004**, *16*, 4452–4466; b) F. J. M. Hoeben, P. Jonkheijm, E. W. Meijer, A. P. H. J. Schenning, *Chem. Rev.* **2005**, *105*, 1491–1546.
- [20] X. H. Sun, C. S. Chan, M. S. Wong, W. Y. Wong, *Tetrahedron* **2006**, *62*, 7846–7853.

- [21] a) G. W. Gray, J. W. G. Goodby, *Smectic Liquid Crystals, Textures and Structures*, Leonard Hill, Glasgow, **1984**; b) I. Dierking, *Textures of Liquid Crystals*, Wiley-VCH, Weinheim, **2003**.
- [22] a) C. Noël in *Polymeric Liquid Crystals* (Ed.: A. Blumstein), Plenum Press, New York, **1985**, pp. 21–63; b) A. P. H. J. Schenning, A. F. M. Kilbinger, F. Biscarini, M. Cavallini, H. J. Cooper, P. J. Derrick, W. J. Feast, R. Lazzaroni, Ph. Leclère, L. A. McDonell, E. W. Meijer, S. C. J. Meskers, *J. Am. Chem. Soc.* **2002**, *124*, 1269–1275.
- [23] T. Sekine, T. Niori, J. Watanabe, T. Furukawa, S. W. Choi, H. Takezoe, *J. Mater. Chem.* **1997**, *7*, 1307–1309.
- [24] P. K. Lo, D. Z. Chen, Q. W. Meng, M. S. Wong, *Chem. Mater.* **2006**, *18*, 3924–3930.
- [25] a) Y. Yoon, R. M. Ho, F. M. Li, M. E. Leland, J. Y. Park, S. Z. D. Cheng, V. Percec, P. W. Chu, *Prog. Polym. Sci.* **1997**, *22*, 765–794; b) W. R. Krigbaum, J. Watanabe, T. Ishikawa, *Macromolecules* **1983**, *16*, 1271–1279; c) F. Mathevet, P. Masson, J. F. Nicoud, A. Skoulios, *J. Am. Chem. Soc.* **2005**, *127*, 9053–9061.
- [26] J. Thisayukta, Y. Nakayama, S. Kawauchi, H. Takezoe, J. Watanabe, *J. Am. Chem. Soc.* **2000**, *122*, 7441–7448.
- [27] M. Hird, J. W. Goodby, N. Gough, K. J. Toyne, *J. Mater. Chem.* **2001**, *11*, 2732–2742.
- [28] S. A. Lee, S. Hotta, F. Nakanishi, *J. Phys. Chem. A* **2000**, *104*, 1827–1833.
- [29] S. Westenhoff, A. Abrusci, W. J. Feast, O. Henze, A. F. M. Kilbinger, A. P. H. J. Schenning, C. Silva, *Adv. Mater.* **2006**, *18*, 1281–1285.
- [30] H. Goto, Y. Okamoto, E. Yashima, *Macromolecules* **2002**, *35*, 4590–4601.
- [31] B. M. W. Langeveld-Voss, R. A. J. Janssen, E. W. Meijer, *J. Mol. Struct.* **2000**, *521*, 285–301.
- [32] A. Mucci, F. Parenti, R. Cagnoli, R. Benassi, A. Passalacqua, L. Preti, L. Schenetti, *Macromolecules* **2006**, *39*, 8293–8302.
- [33] M. Melucci, G. Barbarella, M. Gazzano, M. Cavallini, F. Biscarini, A. Bongini, F. Piccinelli, M. Monari, M. Bandini, A. Umani-Ronchi, P. Biscarini, *Chem. Eur. J.* **2006**, *12*, 7304–7312.
- [34] J. Thisayukta, H. Niwano, H. Takezoe, J. Watanabe, *J. Am. Chem. Soc.* **2002**, *124*, 3354–3358.
- [35] T. Sanji, N. Kato, M. Tanaka, *Chem. Asian J.* **2008**, *3*, 46–50.
- [36] D. M. Walba, E. Korblova, C. C. Huang, R. Shao, M. Nakata, N. A. Clark, *J. Am. Chem. Soc.* **2006**, *128*, 5318–5319.
- [37] T. J. Dingemans, N. S. Murthy, E. T. Samulski, *J. Phys. Chem. B* **2001**, *105*, 8845–8860.
- [38] a) B. Das, S. Grande, W. Weissflog, A. Eremin, M. W. Schröder, G. Pelzl, S. Diele, H. Kresse, *Liquid Crystals* **2003**, *30*, 529–539; b) R. Stannarius, J. Li, W. Weissflog, *Phys. Rev. Lett.* **2003**, *90*, 025502.
- [39] P. T. Boudreault, S. Wakim, N. Blouin, M. Simard, C. Tessier, Y. Tao, M. Leclerc, *J. Am. Chem. Soc.* **2007**, *129*, 9125–9136.

Received: November 26, 2008  
Published online: February 13, 2009